International Journal of Thermophysics (2022) 43:177
https://doi.org/10.1007/s10765-022-03101-1

Mutual Diffusivities of Binary Mixtures of Water and Poly(ethylene) Glycol from Heterodyne Dynamic Light Scattering

Wenchang Wu[1] · Malvina Supper[2] · Michael H. Rausch[1] · Malte Kaspereit[2] · Andreas P. Fröba[1]

Received: 17 August 2022 / Accepted: 7 September 2022 / Published online: 5 October 2022

Abstract

In the present study, the mutual diffusivity D_{11} in binary mixtures of water with technical polydisperse poly(ethylene) glycol (PEG) blends with molar masses of (1000, 4000, or 6000) g·mol^{-1} as well as with a purified monodisperse PEG homolog with a polymerization number of 21 and a molar mass of 943 g·mol^{-1} was investigated by heterodyne dynamic light scattering (DLS) as a function of temperature and/or PEG concentration. The measured D_{11} for technical PEG 1000 and pure PEG 943 match within the experimental uncertainties and agree well with the available literature data. D_{11} decreases with increasing molar mass of the PEGs at constant temperature and weight fraction. For the technical PEG 4000, it could be shown that D_{11} increases with increasing temperature and exhibits a nonlinear concentration dependence. This study demonstrates that heterodyne DLS can be applied for the reliable determination of D_{11} of aqueous solutions of PEGs over a broad range of PEG weight fractions from 0.01 up to the solubility limit with an average expanded uncertainty ($k=2$) of 5.5 %. Moreover, the results show that monodisperse PEGs are suitable model systems for studying the diffusion behavior of bimodal and also multimodal particulate systems.

Keywords Chromatography · Dynamic light scattering · Monodisperse · Mutual diffusivity · Poly(ethylene) glycol

✉ Andreas P. Fröba
andreas.p.froeba@fau.de

[1] Department of Chemical and Biological Engineering (CBI) and Erlangen Graduate School in Advanced Optical Technologies (SAOT), Institute of Advanced Optical Technologies – Thermophysical Properties (AOT-TP), Friedrich-Alexander-Universität Erlangen-Nürnberg (FAU), Paul-Gordan-Straße 8, 91052 Erlangen, Germany

[2] Department of Chemical and Biological Engineering (CBI), Institute for Separation Science & Technology (TVT), Friedrich-Alexander Universität Erlangen-Nürnberg (FAU), Egerlandstraße 3, 91058 Erlangen, Germany

1 Introduction

Poly(ethylene) glycol (PEG) is a hydrophilic polymer described by the molecular formula H–[O–CH_2–CH_2]$_n$–OH representing the repeating ethylene oxide unit –[O–CH_2–CH_2]–. The polymerization number n defines the number of repeating units in the molecule and, thus, the chain length related to the molar mass of the PEG. A PEG system can be referred to as monodisperse or pure if it only consists of PEG molecules with one defined n. On the contrary and describing its most commonly used form, a PEG system is called polydisperse or technical if it consists of PEG molecules within a range of n, resulting in a Gaussian distribution of the molar mass with a central averaged molar mass, often denoted as M_n.

There are various applications of PEGs benefiting from their high solubility in water, nontoxicity, low volatility, biodegradability as well as their chemical and microbiological inertness [1]. PEGs can be used in pharmaceutical, chemical, cosmetic, and food industries, e.g., as drug delivery systems [2] or for protein modifications [3, 4]. They have also been widely employed as environmentally friendly alternative solvent [5–8]. In all these applications, polydisperse PEGs are ubiquitously used due to their low cost. However, the importance of monodisperse PEGs and their derivatives is rapidly increasing, especially in clinical applications where monodisperse PEG-based drug products simplify the purification, characterization, and quality control [9, 10]. In addition, monodisperse PEGs possess well-defined properties which are needed for analytical standards for chromatography. In such applications, a precise knowledge of their thermophysical properties including transport properties is required for both the technical and pure PEGs. In connection with diffusivities studied here, Vergara et al. [11] reported mutual diffusion coefficients D_{11} in aqueous solutions of technical PEGs determined by Gouy interferometry. The self-diffusivity D_1 of monodisperse PEG oligomers with $n = (1$ to $40)$ was measured in dilute solutions of deuterium oxide (D_2O) by pulsed-field gradient nuclear magnetic resonance by Shimada et al. [12]. Moreover, diffusivities of technical PEG aqueous solutions by dynamic light scattering (DLS) have been reported by Feitosa et al. [13]. A similar investigation by DLS has been reported in Ref. [14], however, with focus on the determination of the size of the dissolved PEG molecules. To the best of our knowledge, DLS investigations for pure PEG systems are not available in the literature. So far, this rather scarce data situation hinders the development of a clear picture on the general behavior and similarities of diffusivities of technical and pure PEGs.

Due to the nature of long-chained PEG molecules, they tend to form individual sphere-like folded coils in solution [15, 16]. Such solutions resemble dispersions of spherical particles where the individual PEG molecules could be understood as extremely small nanoparticles. For such a solution close to infinite dilution of PEG, the mutual diffusivity D_{11} can be related to the self-diffusivity of sphere-like PEG molecules with a specific hydrodynamic diameter d_H. Therefore, solutions of monodisperse PEG molecules can be considered as model systems to gain a fundamental understanding of diffusive processes in particulate systems, including bimodal and also multimodal systems. Here, the major advantage of

using monodisperse PEGs is that their polydispersity index in size is much closer to a value of zero in comparison with other nanoparticle samples.

In the present work, the applicability of heterodyne DLS for the determination of the mutual diffusivity D_{11} of aqueous PEG systems will be demonstrated first. Then, measured D_{11} of binary solutions containing water and technical polydisperse PEGs with $M_n = (1000, 4000, \text{or } 6000)$ g·mol^{-1} as well as with pure monodisperse PEG with polymerization number $n = 21$ and molar mass $M = 943$ g·mol^{-1} for temperatures T from (288 to 348) K and for PEG mass fractions from 0.001 and approaching the solubility limit are reported and discussed. This also includes a comparison of the measured D_{11} for the technical PEG 1000 and the pure PEG 943 systems in terms of experimental uncertainties.

2 Experimental Section

2.1 Materials and Sample Preparation

The technical PEG 1000 (CAS-No. 25322-68-3, $M_n = 1000$ g·mol^{-1}) and PEG 4000 (CAS-No. 25322-68-3, $M_n = 4000$ g·mol^{-1}) investigated in the present work were purchased from Merck KGaA. Technical PEG 6000 (CAS-No. 25322-68-3, $M_n = 6000$ g·mol^{-1}) was purchased from VWR Chemicals. They all are solid flakes at about 293 K and their purities are not specified by the supplier. The monodisperse pure PEG 943 homolog with a polymerization number of $n = 21$ ($M = 943$ g·mol^{-1}) was produced from the technical PEG 1000 based on reversed-phase chromatography. Detailed description of the synthesis can be found as follows.

The pure homolog was fractionated out of a polydisperse technical PEG 1000 sample. The molar mass distribution of the latter obtained by liquid chromatography/mass spectrometry (LC/MS) [17] consists of 20 detectable different polymerization degrees. The pure sample was obtained by reversed-phase semi-preparative liquid chromatography using a core–shell column (Kinetex C18, 100 × 21 mm, 100 Å, 5 µm; Phenomenex). Detection was performed by a charged aerosol detector (Corona Ultra RS, Thermo Fisher Scientific). A modular setup with gradient pump, thermostat, fraction collector and charged aerosol detection (CAD) coupled with MS detection was implemented and controlled by a Python-based software. The injection volume was 50 µl at a concentration of 250 g·kg^{-1} using a flow rate of 20 ml·min^{-1}. The temperature of the thermostat (RE 306, Lauda) to control column temperature was set to 328 K. The eluent was a mixture of acetonitrile and water. A linear gradient starting from 15 % to 18 % of acetonitrile in 70 min was applied while still achieving base line separation. The eluting PEG homologs were identified based on their molar mass using a mass spectrometer (ABI SciexQTrap, Sciex) and peaks were collected by fraction collector (Foxy R1, Knauer). Repetitive runs for polydisperse PEG samples delivered pure single homologs with different degrees of polymerization. Between the individual experiments a forced elution step using a volume concentration of 50 % acetonitrile was performed to flush out larger PEGs that were still residing in the column. Data acquisition and processing was performed using the softwares Chromeleon 6.80 (Dionex) and Analyst (Sciex). In

the present work, monodisperse PEG 943 is considered as a purified equivalent to the technical PEG 1000. Deionized water produced from tap water was used for the preparation of the aqueous PEG solutions without further purification.

All binary mixtures containing water and one PEG type were prepared gravimetrically by means of an analytical balance with a specified precision of 0.1 mg, where an absolute expanded ($k=2$) measurement uncertainty of 1 mg was estimated. The latter results in an average expanded relative uncertainty of 7.2 % for the PEG weight fraction w_{PEG} for mixtures with $w_{\mathrm{PEG}}=0.001$ and reduces to 0.7 % for mixtures with high w_{PEG}. To ensure mixture homogeneity, all prepared mixtures were stirred with help of a magnetic stirrer for at least 20 min. A summary of all mixture compositions is given in Table 1, where the refractive indices of the samples are also given.

2.2 Analytical Chromatography

The purity of the fractionated sample was confirmed at analytical scale by LC/MS using a core–shell column with high separation efficiency (Kinetex C18, 100×4.6 mm, 100 Å, 2.6 µm; Phenomenex) and a Ultimate 3000 LC unit (Dionex) consisting of a gradient pump LPG-3400A with internal degasser, column thermostat TCC-3000, and an autosampler WPS-3000SL. Detection was performed by a charged aerosol detector (Corona Ultra RS, Thermo Fisher Scientific). Isocratic measurements with an acetonitrile volume content of 20 % and a temperature of 298 K were performed. A volume of 10 µL was injected at a flow rate of 1 $\mathrm{ml\cdot min^{-1}}$. For comparison, the original technical PEG 1000 was additionally measured at a concentration of 1 $\mathrm{g\cdot l^{-1}}$ using the same conditions as for the fractions.

2.3 Heterodyne Dynamic Light Scattering (DLS)

For molecular binary systems such as liquids containing a dissolved gas, DLS has proven to allow the accurate and simultaneous determination of mutual diffusivity D_{11} and thermal diffusivity a in an absolute way [18–21]. The same also holds true for the determination of the translational particle diffusion coefficient D_{T} in free media and under confinement in particulate systems consisting of isotropic particles dispersed in liquids [22] as well as of D_{T} and the rotational particle diffusion coefficient D_{R} in dispersions containing anisotropic particles [23]. In contrast to conventional techniques, DLS does not require a calibration and is applied in macroscopic thermodynamic equilibrium. Thus, no macroscopic gradient, which may cause advection, has to be applied. The fundamentals and the application of the DLS method within thermophysical property research [24, 25] have been described in detail in the example literature sources cited above. In the following, only essential information about the method and the experimental realization in the present study is given.

When a bulk fluid sample in macroscopic thermodynamic equilibrium is irradiated by coherent laser light, scattered light from the sample can be observed in all directions. The underlying scattering process is governed by statistical microscopic fluctuations in temperature or entropy, in pressure, and in species concentration in

Table 1 Refractive index n_D at the central wavelength of the sodium line ($\lambda_D = 589.3$ nm) as well as the principal dispersion $n_F - n_C$ for the Fraunhofer lines ($\lambda_F = 486.1$ nm and $\lambda_C = 656.3$ nm) determined with an Abbe refractometer as function of T and/or w_{PEG}

T/K	w_{PEG}	n_D	$n_F - n_C$
PEG 1000			
298.2	0.001	1.3326	0.0047
298.1	0.010	1.3337	0.0055
PEG 4000			
288.2	0.001	1.3338	0.0050
288.2	0.010	1.3346	0.0052
298.2	0.001	1.3327	0.0043
298.2	0.010	1.3339	0.0057
298.2	0.050	1.3390	0.0046
298.1	0.100	1.3460	0.0043
298.1	0.100	1.3460	0.0043
298.1	0.200	1.3602	0.0056
298.1	0.300	1.3756	0.0051
298.1	0.300	1.3756	0.0051
298.2	0.398	1.3905	0.0066
298.2	0.500	1.4055	0.0065
298.1	0.599	1.4218	0.0061
308.2	0.001	1.3311	0.0045
308.2	0.010	1.3322	0.0057
318.2	0.010	1.3309	0.0071
328.1	0.010	1.3290	0.0062
338.2	0.010	1.3271	0.0060
348.1	0.010	1.3244	0.0061
PEG 6000			
298.3	0.001	1.3326	0.0033
298.1	0.010	1.3339	0.0044

Uncertainties for n_D and T as specified by the manufacturer are $U(n_D) = 0.0002$ and $U(T) = 0.2$ K. Absolute uncertainties for $n_F - n_C$ are $U(n_F - n_C) = 0.0024$. Estimated uncertainties for w_{PEG} vary between $U_r(w_{PEG}) = (0.02$ and $8.7)$ % for $w_{PEG} = (0.6$ to $0.001)$ with an average of 1.8 %. All uncertainties are given on a confidence level of 0.95

mixtures. By analyzing the temporal behavior of the scattered light intensity and, thus, the relaxation of these statistical fluctuations following the same laws as the equilibration of gradients in macroscopic systems [26], the DLS method allows the absolute determination of multiple thermophysical properties. In the case of a binary mixture and neglecting pressure fluctuations by focusing only on the Rayleigh components of the scattered light, information about the dissipation processes of the temperature and concentration fluctuations can be derived by the temporal analysis of the scattered light intensity by calculating the second-order correlation function (CF). In DLS experiments using a heterodyne detection scheme, the scattered light from the sample fluid is coherently superimposed with a reference light, also called

local oscillator, of a much larger intensity. The reference light can be generated in a defined way or be present from further scattering processes in the optical path, e.g., from the windows of the sample container as well as from the inside of the sample. In the heterodyne case, the recorded normalized intensity CF takes the form

$$g^{(2)}(\tau) = a_0 + b_\mathrm{t} \exp\left(-\frac{|\tau|}{\tau_\mathrm{C,t}}\right) + b_\mathrm{c} \exp\left(-\frac{|\tau|}{\tau_\mathrm{C,c}}\right), \tag{1}$$

where the experimental constants a_0, b_t, and b_c are defined by the characteristics of the experimental setup, the statics of the fluctuations in temperature and concentration at a given thermodynamic state, and the strength of the local oscillator field. $\tau_\mathrm{C,t}$ and $\tau_\mathrm{C,c}$ are the mean lifetimes of fluctuations in temperature and concentration, and are linked to the thermal diffusivity a and the mutual diffusivity D_{11} by

$$a = \frac{1}{\tau_\mathrm{C,t} q^2} \tag{2}$$

and

$$D_{11} = \frac{1}{\tau_\mathrm{C,c} q^2}. \tag{3}$$

Here,

$$q = \frac{4\pi n_\mathrm{fluid}}{\lambda_0} \sin\left(\frac{\Theta_\mathrm{S}}{2}\right) \tag{4}$$

is the modulus of the scattering vector for a given fluid sample with the refractive index n_fluid at the laser wavelength in vacuo λ_0. The scattering angle Θ_S inside the sample is determined via the Snell–Descartes law using n_fluid and the incident angle Θ_i defined by the directions of the incident light outside the sample container and that of the scattered light. Due to the direct connection between the observed mean lifetimes of fluctuations and q, diffusive processes on the order of (10^{-13} to 10^{-10}) $\mathrm{m^2 \cdot s^{-1}}$ are analyzed at large q values with the optical configuration used in the present study. Therefore, a, which is typically on the order of 10^{-8} $\mathrm{m^2 \cdot s^{-1}}$, is not accessible here. In this case, the normalized intensity CF reduces to

$$g^{(2)}(\tau) = a_0 + b_\mathrm{c} \exp\left(-\frac{|\tau|}{\tau_\mathrm{C,c}}\right). \tag{5}$$

While for small Θ_S values, n_fluid has a negligible influence on the obtained diffusivities, at large values of Θ_S, n_fluid becomes a significant quantity and was therefore also determined in the present work, cf. Sect. 2.4.

The sketch of the optical and electronic arrangement of the DLS setup used in the present work is shown in Fig. 1. Single-mode continuous wave fiber lasers with $\lambda_0 = (488 \text{ or } 532)$ nm were used as light sources. The laser light is directed and focused via a set of mirrors (M) and a lens (L) with a focal length of 2 m into the sample cell represented by the cuvette holder (CH).

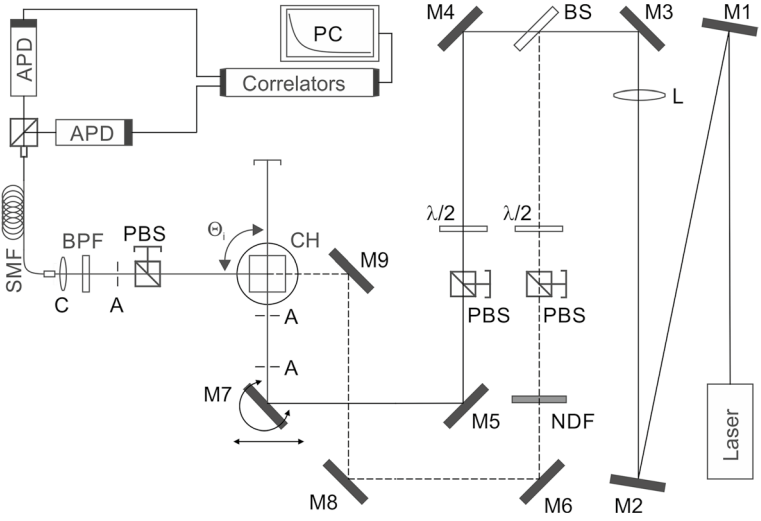

Fig. 1 Arrangement of the optical and electronic components of the setup for DLS experiments

The incident laser beam is split by a beam splitter (BS) into a main beam and a reference beam represented by the solid and the dashed lines. With the reference beam, the alignment of the detection direction and the heterodyne detection scheme are realized. To achieve the latter, the reference beam is coherently superimposed to the scattered light. The intensity and polarization of both the main beam and the reference beam are controlled using combinations of a half-wave plate ($\lambda/2$) and a polarization beam splitter (PBS) being aligned so that only vertically polarized light is transmitted. For the reference light, a neutral density filter (NDF) was additionally inserted into the beam path to further reduce its intensity. The detection direction of the scattered light is fixed by the combination of an aperture (A) and the collimator (C) of a single-mode fiber (SMF) mounted on a 3-axis translational stage. In the first step, the optical setup is adjusted by aligning the main and reference beams so that their reflected beams from the cuvette are in their directions of incidence. This yields an incident angle of $\Theta_i = 90°$. The collimator is adjusted until the maximum intensity is observed from the fiber output. In a second step, with help of a rotational stage carrying mirror M7, the desired incident angle is adjusted relative to the reference value. The uncertainty in Θ_i is estimated by the double maximum resolution of the rotational stage being 0.04°. The scattered light is collected by the collimator and fed into the SMF connected to a fiber splitter which equally splits the scattered light to two avalanche photodiodes (APDs) operated in a pseudo cross-correlation scheme which limits afterpulsing and dead-time effects. To ensure that only scattered and reference light as well as vertically polarized light are detected by the APDs, a band-pass filter (BPF) centered at the employed λ_0 and a further PBS are placed in front of the collimator. The dynamics of the scattered light intensity is temporally resolved by the two APDs. Their pulses are discriminated, amplified, and fed into two different digital correlators. The linear-tau correlator (LTC) features 2047 equally

spaced correlation channels with adjustable interval time or sample time Δt. The multiple-tau correlator (MTC) has 263 channels with a fixed but broader quasi-logarithmic time structure, i.e., Δt is increased with increasing lag time. While the MTC can provide a scan of all signals present at very short up to very large time scales, the LTC gives the highest temporal resolution for the time range of interest by selecting a suitable Δt. To avoid disturbances rising from laser heating, the incident laser power measured at the incident beam inlet to the cuvette holder is limited to 47 mW. The power of the reference beam is only a few μW and below. Preliminary studies have shown no influence of the adjusted laser power in the applied range on the obtained D_{11}.

The aluminum core of the temperature-controlled cuvette holder features four optical accesses covering both sides of the cuvette. This design combined with the optical arrangement allows the analysis of the scattered light for $\Theta_i = (70 \text{ to } 110)°$, where $\Theta_i = (70 \text{ to } 90)°$ were adjusted in the present study due to temporal resolution limitations of the used detectors at larger angles combined with the properties of the probed samples. A quartz glass cuvette with a cross section of 10×10 mm^2 and a total volume of 3.5 ml is positioned and sealed in the center of the core part of the cuvette holder by two flanges with protrusions and embedded O-rings. The entire core is wrapped with resistance heating wires (RW) and is further enclosed by a stainless-steel casing with inner liquid channels. The temperatures of the aluminum core, the fluid in the cuvette, and the casing are measured by two calibrated Pt100 resistance probes (Pt1 and Pt2) with an expanded absolute uncertainty ($k = 2$) of 20 mK and one uncalibrated Pt100 (Pt3), respectively, using a millikelvin thermometer. The temperature measured with Pt1 is used in a PID algorithm to regulate the temperature of the core in combination of a digital-to-analog converter, a self-constructed heating amplifier, and a RW. In addition, a laboratory thermostat connected to the liquid circuits in the outer casing is used to control the ambient T. The average stability of the sample temperature measured with Pt2 inside the cuvette is 0.7 mK, which is quantified by the double standard deviation of the temperatures measured within one measurement series typically lasting 1.5 h. The reported T in the figures and tables for the DLS experiments represent the mean values of the data recorded by Pt2 during one complete measurement series.

For each sample and state point, at least 3 individual measurements were performed with different Θ_i, resulting in at least 6 final CFs from the LTC and the MTC altogether. Here, each final CF is the result of averaging multiple CFs with adjusted short integration time recorded within one measurement. For an individual measurement in this work, the number of CFs is (60 or 600) with typical integration time of (10 or 1) s. Thus, the total integration time or total experimental run time is constantly 10 min. For samples with low w_{PEG}, e.g., of 0.01 and 0.001, the scattering originating from the fluctuations in concentration is extremely weak. Therefore, larger integration times were used to achieve sufficient signal-to-noise ratios (SNR) in the CFs. The described "multi-run" scheme is especially beneficial for DLS experiments encountering irregular fluctuations in the count rate, which result in pronounced disturbances in the long-term range of the recorded CFs [27]. Such irregularities may be caused by impurities, e.g., in form of particle contaminations crossing the scattering volume. By recording multiple CFs with short integration

time, individual CFs which are affected by irregular count rate fluctuations can easily be discarded in the data evaluation procedure.

From the many CFs obtained in one measurement with the same incident angle, correlator, and thermodynamic state, one averaged CF is calculated using a post-processing algorithm. The applied data evaluation procedure is similar to the one detailed in our previous studies [28, 29]. The averaged experimental CFs are fitted by nonlinear regression to find the experimental constants and the mean lifetimes of fluctuations in concentration $\tau_{C,c}$ with the appropriate theoretical model based on Eq. 5. Two typical experimental averaged CFs are shown in Fig. 2.

For the probed aqueous solutions of the pure PEG 943 homolog with $w_{PEG} = 0.01$ and technical PEG 4000 with $w_{PEG} = 0.05$, the experimental CFs obtained under a heterodyne detection scheme can be appropriately described by a single exponential characterizing the dynamics of fluctuations in concentration and an additional first- or second polynomial term. In some cases, however, a second exponential appeared in the experimental CFs and its contribution is more pronounced at low w_{PEG} and normally has a decay time of around 1500 µs, which is at least 150 times larger than the one of the exponential associated with the mass diffusion of PEG molecules. The origin of the second exponential is expected to be related to particle or dust contaminations present in the solid PEG samples. This has been confirmed by the observation of a second exponential in the CFs for two solutions of PEG 4000 prepared with unfiltered and filtered deionized water. Filtration of the mixtures was avoided to prevent possible changes of the PEG concentration. Compared to the weak scattering at

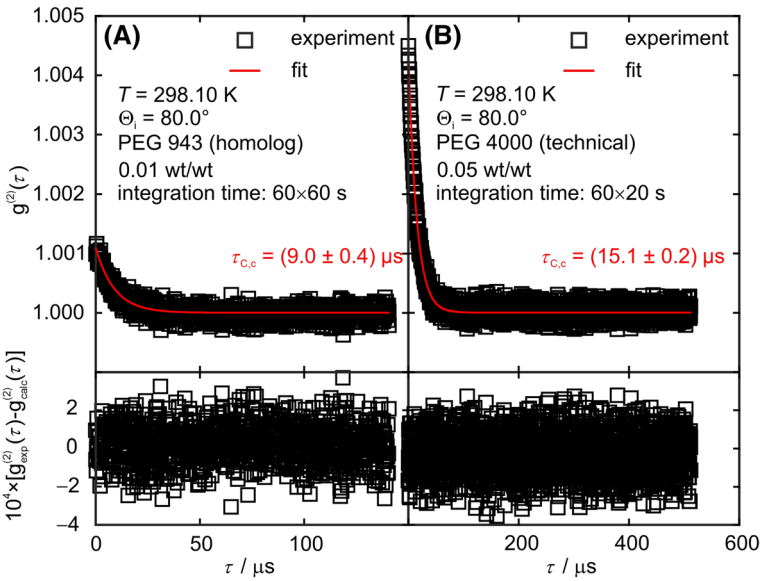

Fig. 2 Upper part: fit to averaged CFs obtained with the STC using a heterodyne detection scheme for aqueous solutions of (A) pure PEG 943 homolog with $w_{PEG} = 0.01$ and (B) technical PEG 4000 with $w_{PEG} = 0.05$. For the averaged CFs, 60 individual CFs with a single integration time of (60 or 20) s are considered. Lower part: absolute residuals of the measured CF from the fit

fluctuations on a molecular level, large contaminating particles in the solution scatter much more strongly, where the scattering intensity scales to the power of six of the particle diameter. Since the decay times of these two exponentials are temporally separated and the sample time of the LTC is always adjusted in a way that maximum temporal resolution of the first exponential is achieved, the second exponential can be well described by either a first- or a second-order polynomial in addition to the mathematical model shown in Eq. 5. In this case, any influences on the fitted decay time $\tau_{C,c}$ and, thus, on D_{11} can be neglected. For clarity purposes, Fig. 2 shows the CFs after subtracting the long-term decay and, thus, the disturbances from the originally measured CFs. In all measurements of the present study, the fit was considered to be appropriate only if the residuals, i.e., the differences between the experimental data and the corresponding fit, were free of any systematic behaviors as given for the examples in Fig. 2. As expected, the SNR of the CF generally increases with increasing w_{PEG} and allows to achieve lower fitting uncertainties even if the total integration time is clearly increased for small w_{PEG}.

According to Eqs. 3 and 4, D_{11} is obtained from the fitted mean lifetimes of the fluctuations in concentration, the details on the optical arrangement, and the refractive index of the fluid at the laser wavelength applied in the DLS experiment. The reported D_{11} data for a defined mixture and thermodynamic state were determined by averaging the individual results for D_{11} from all averaged CFs obtained with the LTC and the MTC in one measurement series, where a weighting scheme based on the inverse relative uncertainties of the individual D_{11} data was applied. The latter uncertainties are given on a level of confidence of 0.95 ($k=2$) and were determined by uncertainty propagation calculations accounting for the statistical uncertainty in the fitting of the CF as well as in the experimental uncertainties in n_{fluid} and Θ_i.

2.4 Measurement of the Refractive Index

As evident from the definition of the modulus of the scattering vector q, cf. Sect. 2.3, the refractive index of the mixtures, n_{fluid}, at the laser wavelength λ_0 applied in DLS experiments is required for their evaluation. To allow for the determination of n_{fluid}, refractive indices n_D at the central wavelength of the sodium line ($\lambda_D=589.3$ nm) as well as the principal dispersion $n_F - n_C$ for the Fraunhofer lines ($\lambda_F=486.1$ nm and $\lambda_C=656.3$ nm) were measured with an Abbe refractometer by five consecutive measurements. The temperatures for the refractive index measurements were adjusted as close as possible to those investigated in DLS experiments using a laboratory thermostat and measured by the refractometer's internal digital thermometer. For the latter, the absolute specified uncertainty is 0.2 K. While the resulting absolute expanded uncertainty ($k=2$) in the measurement of n_D is specified by the manufacturer to be 0.0002, the corresponding uncertainty of $n_F - n_C$ for every sample and thermodynamic state is estimated to be 0.0024 by propagating the errors of the associated quantities, which are quantified by their double standard deviations within five consecutive measurements.

3 Results and Discussion

In this work, four series of binary mixtures containing deionized water and technical PEG 1000, technical PEG 4000, technical PEG 6000, or the monodisperse PEG 943 homolog were studied by DLS. The aqueous solution of pure PEG 943 was also investigated by analytical chromatography, where the corresponding results are shown first. Then, the measured refractive index data of the samples studied by DLS are presented. The DLS results will finally be discussed regarding the dependences of D_{11} on the molar mass of the PEGs, on the concentration of technical PEG 4000 at constant temperature, and on temperature for a mixture with technical PEG 4000 close to infinite dilution.

3.1 Analysis of the Sample Purity

To verify the purity of the produced monodisperse PEG 943, fractions of preparative runs were analyzed using analytical LC/MS. The experimental settings are described above in Sect. 2.2. A typical preparative run and the corresponding analytical results of the fraction can be seen in Fig. 3. The fractionation time was highlighted in green in Fig. 3A. The collected liquid was subsequently analyzed analytically as indicated by the green solid line in Fig. 1B in comparison to the original PEG 1000 sample as indicated by the black dotted line in the same figure. In the fraction, no other oligomers were detected above the quantitation limit but PEG 943. The subfigure in Fig. 3B shows the proportion of the PEG molecules with different degree of polymerizations determined by LC/MS, where the target homolog, PEG 943, is marked in green. When high purity was confirmed, the liquid of the fraction was reduced by vacuum rotary evaporator and subsequently freeze-dried to powder form.

3.2 Refractive Index

The measured refractive index data n_D as well as the principal dispersions $n_F - n_C$ are listed in Table 1. For the calculation of q required in the evaluation of the DLS measurements, the refractive index of the samples n_{fluid} at the corresponding measurement conditions and laser wavelength λ_0 should be used. The refractive index measurements were performed at temperatures deviating less than 0.15 K from those of the corresponding DLS experiments. As this deviation is smaller than the uncertainty of the temperature measured in the Abbe refractometer and as such deviations also affect the resulting D_{11} values much less than the typical fit uncertainties of $\tau_{C,c}$, temperature-related corrections of refractive index data were not performed. To obtain n_{fluid} for a given mixture and temperature at λ_0, the measured n_D and the measured principal dispersion $n_F - n_C$ were thus directly used. From error propagation calculations using the uncertainties given in Sect. 2.4, the resulting average relative expanded uncertainty in n_{fluid} considering in total 23 data points is 0.2 %. As no measurements could be performed for the mixture with monodisperse PEG 943 homolog with $w_{PEG} = 0.01$, the corresponding data for the mixture including the

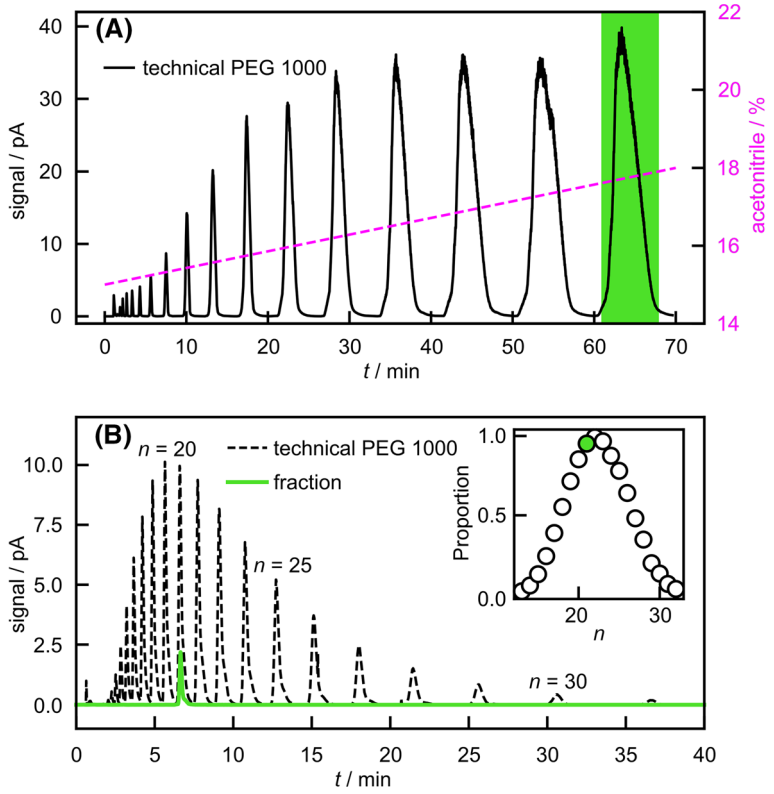

Fig. 3 (A) Representative chromatogram of a preparative run (solid line) with the applied linear gradient of acetonitrile (dashed line), where the fractionation time is highlighted in green. (B) The analytical results of the fractionation of PEG 1000 (solid line) in comparison with the original PEG 1000 sample (dashed line). The subfigure in (B) shows the proportion of the PEG molecules with different polymerizations in the technical PEG 1000 sample (Color figure online)

unpurified technical PEG 1000 with $w_{\mathrm{PEG}} = 0.01$ is used for the evaluation of the DLS experiments.

3.3 Mutual Diffusivity

The mutual diffusivity data obtained from heterodyne DLS and their relative expanded uncertainties ($k = 2$) are summarized in Table 2. Considering all investigated systems and thermodynamic states, the uncertainty in D_{11} ranges from (1.4 to 46.7) % and is 10.3 % on average. For systems with $w_{\mathrm{PEG}} \geq 0.01$, the maximum and the average uncertainties in D_{11} reduce to 13.0 % and 5.5 % The uncertainties of D_{11} decrease with increasing w_{PEG} because of the increasing scattering intensity originating from the fluctuations in concentration. This results in higher SNR in the experimental CFs and, thus, in lower fitting uncertainties and more reliably determined D_{11} values.

Table 2 Mutual diffusivity D_{11} and its relative expanded uncertainty ($k=2$) determined by heterodyne DLS for the investigated aqueous solutions of PEGs as a function of T and/or weight fraction of PEG w_{PEG}

T/K	w_{PEG}	$10^9 \times D_{11}/(m^2 \cdot s^{-1})$	$100 \times U_r\,(D_{11})$
PEG 943			
298.10	0.010	0.266	11.7
PEG 1000			
298.10	0.001	0.197	46.7
298.10	0.010	0.261	9.5
PEG 4000			
288.17	0.001	0.098	18.2
288.16	0.010	0.101	5.1
298.11	0.001	0.122	14.3
298.10	0.010	0.131	7.0
298.10	0.050	0.151	3.1
298.17	0.100	0.172[a]	3.2
298.20	0.100	0.173[a,b]	1.4
298.17	0.200	0.204[a,b]	2.0
298.17	0.200	0.208	2.9
298.19	0.300	0.236[a,c]	7.8
298.10	0.300	0.233	2.1
298.15	0.398	0.239[a]	2.7
298.18	0.500	0.220[a]	2.8
298.13	0.599	0.154[a]	13.3
307.99	0.001	0.184	34.1
307.98	0.010	0.174	8.0
317.98	0.010	0.211[a]	3.7
328.09	0.010	0.254[a]	4.3
338.15	0.010	0.310[a]	4.7
348.12	0.010	0.357[a]	4.6
PEG 6000			
298.11	0.001	0.105	14.5
298.10	0.010	0.110	5.6

Uncertainty for the sample temperature is $U(T)=20$ mK. The estimated relative uncertainties for w_{PEG} vary between $U_r(w_{PEG})=(0.02$ and 8.7) % with an average of 1.8 %. The uncertainties are given on a confidence level of 0.95

[a]Measurement was performed with a laser with $\lambda_0=488$ nm

[b]Repetition measurement with filtered sample

[c]Repetition measurement with the original sample

3.3.1 Dependence on Molar Mass of PEGs at Infinite Dilution

The D_{11} data in binary mixtures containing water and technical or pure PEGs close to their infinite dilution determined by heterodyne DLS at a mean temperature of $T=298.1$ K are shown as a function of the molar mass M of PEGs in Fig. 4. Here, solutions with $w_{PEG}=(0.001$ and $0.01)$ were investigated to be in the vicinity of

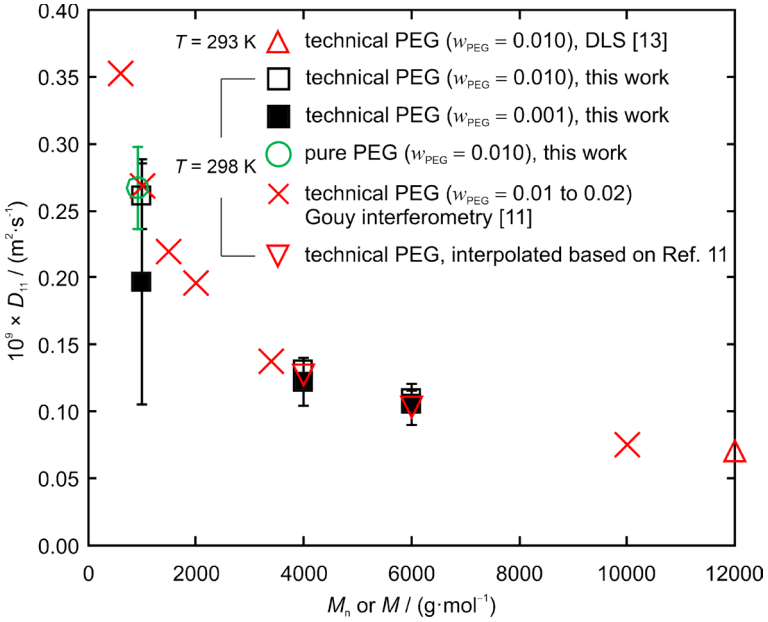

Fig. 4 Mutual diffusivity D_{11} in binary mixtures of water and technical or pure PEGs determined in the vicinity of infinite dilution as a function of the molar mass M_n or M of PEG. Expanded experimental uncertainties ($k=2$) by DLS experiments are indicated by error bars

infinite dilution of the solute PEG. In this regime, the mutual diffusivity D_{11} and the self-diffusivity of the solute D_1 match and are equal to the tracer diffusion coefficient of the solute [29]. As described in the introduction section, D_{11} can also be related to the self-diffusivity of the sphere-like PEG molecules with a specific hydrodynamic diameter d_H dispersed in the solution.

Figure 4 shows that D_{11} in the dilute aqueous solutions of PEGs decreases with increasing molar mass of the PEGs, where this trend is describable by a power function. As expected for this concentration regime, the D_{11} values in solutions of technical PEGs with different w_{PEG} illustrated by open and closed black squares match within their expanded ($k=2$) uncertainties indicated by error bars. The same trend of D_{11} as a function of molar mass of PEGs was reported by Vergara et al. [11], who studied the mutual diffusion coefficients in binary solutions containing water and technical PEGs by Gouy interferometry. Their D_{11} data for PEGs with M_n ranging from (600 to 10,000) g·mol^{-1} are shown by red crosses in Fig. 4. For a better comparison between the values from Ref. [11] and determined by heterodyne DLS, the literature data are additionally interpolated to M_n=(4000 and 6000) g·mol^{-1} based on a description of the complete D_{11} dataset determined close to infinite dilution as a function of M_n by a power function. The interpolated literature data agree very well with the D_{11} or self-diffusivity data close to infinite dilution of the PEGs measured by DLS. A further D_{11} value of 0.07×10^{-9} m^2·s^{-1} in binary solution containing water and technical PEG 12,000 with $w_{PEG}=0.01$ determined by DLS at $T=293$ K from Feitosa et al. [13] is also included in Fig. 4 for comparison. Here, this D_{11}

value is estimated based on the data plot reported in their paper and matches very well with the above-mentioned trend of D_{11} despite the T difference.

One important aspect of the present work is the comparison of D_{11} for aqueous solutions of a technical PEG with a certain distribution of M and a corresponding pure monodisperse PEG homolog, which are technical PEG 1000 and pure PEG 943 here. Due to the limitation in the amount of synthesized pure PEG 943 and in the minimum required volume for the DLS experiments, the corresponding measurements are restricted to $w_{PEG}=0.01$. Figure 4 shows that the two determined D_{11} values agree well with a deviation of 2.2 %, which is clearly within their experimental uncertainties of (9.5 and 11.7) %. From this, it can be concluded that D_{11} determined for a technical aqueous polydisperse PEG system is an averaged value which is similar to the corresponding value for aqueous solutions of pure monodisperse PEGs with $M_{monodisperse} \approx M_{n,polydisperse}$. Although the influence of polydispersity on D_{11} for technical PEGs could not be examined in detail due to the relatively large uncertainties originating from the low PEG concentration, the determined D_{11} values tend to be smaller for technical PEGs compared to the pure one. This might be explained as follows. For a typical technical PEG system, the molar masses of the macromolecules with different degree of polymerization are Gaussian distributed with a central peak at M_n. Assuming the molar mass of a PEG sphere-like molecule and the scattering intensity from it is directly proportional to ${d_H}^3$ and ${d_H}^6$, the distribution of the scattering intensities for a polydisperse system is deformed and shifted to larger particle diameters in comparison to the Gaussian distribution valid for the molar mass. This leads to larger weights for the CFs of the larger molecules. Thus, a larger average decay time and smaller effective D_{11} can be expected for a polydisperse system in comparison to a corresponding monodisperse one.

Assuming a spherical shape of the dissolved PEG molecules, hydrodynamic diameters of PEG 1000 and PEG 6000 of (1.9 and 4.7) nm can be calculated via the Stokes–Einstein equation [30] using the determined D_{11} at $w_{PEG}=0.01$ and the dynamic viscosity of 0.891 mPa·s for the solvent water at $T=298.1$ K from Huber et al. [31]. These values agree well with the viscosity diameters of (1.8 and 4.9) nm calculated based on the correlation proposed in Ref. [32]. In the latter study, the viscosity diameter refers to the diameter of an equivalent sphere in aqueous solution. This may imply that the individual long-chained PEG molecules really take a sphere-like shape and behave similarly to a particulate system.

3.3.2 Dependence on w_{PEG} for Technical PEG 4000

D_{11} of binary mixtures of water and technical PEG 4000 with w_{PEG} ranging from 0.001 to the observed solubility limit of about 0.6 at $T=298$ K determined by heterodyne DLS are shown as a function of w_{PEG} in Fig. 5. There, also literature D_{11} data for aqueous solutions of technical PEG 3400 determined by Gouy interferometry [11], an interpolated D_{11} value for an aqueous solution of technical PEG 4000 close to infinite dilution based on the data given in Ref. [11] as already shown in Fig. 4, and an interpolated value for the self-diffusivity D_1 for an aqueous solution of technical PEG 4000 at infinite dilution are given. The interpolation of the latter datum is based on D_1 values calculated via the Flory

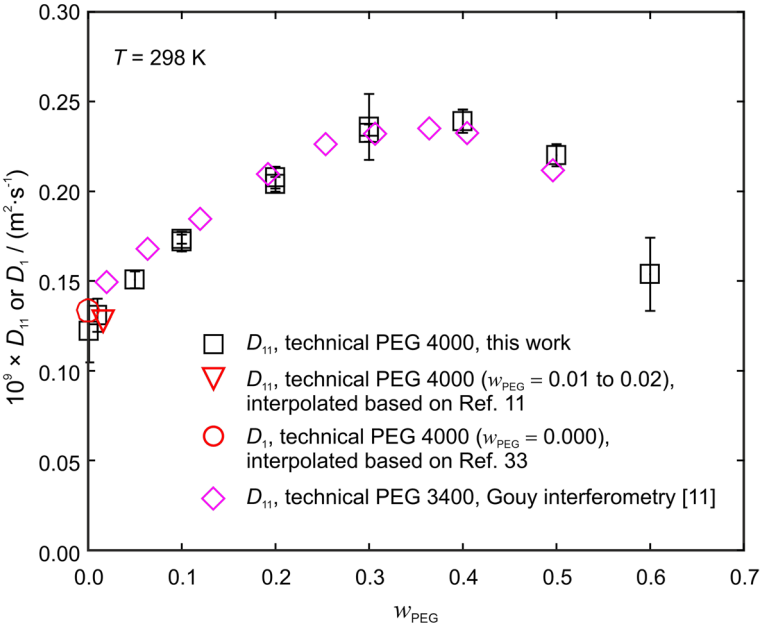

Fig. 5 Mutual diffusivity D_{11} in binary mixtures of water with technical PEG 4000 determined by heterodyne DLS in this work and with technical PEG 3400 determined by Gouy interferometry [11] as a function of w_{PEG} at a mean $T = 298.1$ K. The open downward-pointing triangle represents D_{11} for binary mixtures of water with technical PEG 4000 close to infinite dilution based on the interpolation of D_{11} data given in Ref [11]. The open circle represents the self-diffusivity D_1 of PEG molecules for binary mixtures of water with technical PEG 4000 at infinite dilution based on the interpolation of D_1 data given in Ref. [33]. Expanded experimental uncertainties ($k = 2$) by DLS experiments are indicated by error bars

equation for monodisperse PEGs considering the polydispersity of the technical PEGs as reported in detail in Ref. [33]. This interpolated self-diffusivity D_1 being 0.133×10^{-9} $m^2 \cdot s^{-1}$ at $w_{PEG} = 0.000$ agrees well with the experimental D_{11} value of $(0.131 \pm 0.009) \times 10^{-9}$ $m^2 \cdot s^{-1}$ at $w_{PEG} = 0.010$ from DLS as well as with the interpolated D_{11} value of 0.127×10^{-9} $m^2 \cdot s^{-1}$ at $w_{PEG} =$ (0.01 to 0.02) from Gouy interferometry, demonstrating the convergence of D_{11} and D_1 of the solute close to infinite dilution. At higher w_{PEG}, the data from DLS for PEG 4000 show a pronounced acceleration of the Fick diffusion process by increasing D_{11} values up to $w_{PEG} \approx 0.35$ in spite of the increasing viscosity due to the increasing PEG concentration. The relative increase in D_{11} from the infinite dilution regime to the highest w_{PEG} is nearly 100 %. Then, the diffusive process experiences a strong slowing-down with further increasing w_{PEG} approaching the solubility limit of around 0.6. Almost identical behavior of D_{11} as a function of w_{PEG} in aqueous solutions of technical PEG 3400 was observed by Vergara et al. [11]. Nonlinear concentration-dependent behaviors of D_{11} have been observed for binary mixtures consisting of carbon dioxide dissolved in 1-hexanol [21] or *n*-hexane [34]. In all these works, the non-ideal behavior of the Fick diffusion coefficient close to a change in the phase behavior of the systems studied was attributed to

the contribution from the thermodynamic factor Γ_{11}, which is a structural quantity associated to the molecular organization [21, 34]. In general, the interplay between Γ_{11} and the Maxwell–Stefan diffusion coefficient $Đ_{12}$, which characterizes the hydrodynamic or kinetic contribution of the diffusion process, determines the concentration dependence of D_{11}, $D_{11}=\Gamma_{11}\cdot Đ_{12}$ [11, 21, 34, 35]. For highly non-ideal mixtures like the investigated PEG 4000 system, the contribution of Γ_{11} to D_{11} may become much more significant than $Đ_{12}$. Thus, in our case, D_{11} for the PEG 4000 system follows the concentration dependence of Γ_{11} which shows a maximum at $w_{\mathrm{PEG}} \approx 0.55$, see Ref. [11]. The mismatch of w_{PEG} where the maxima of D_{11} and Γ_{11} are located suggests a further contribution from $Đ_{12}$. The initial increase in Γ_{11} being above unity with increasing w_{PEG} can be related to the large difference in the molecule size between water and PEG molecules. Similar observations have been reported in Ref. [20] and explained in Ref. [36]. In the paper of Vergara et al. [11], it is stated that the decrease in Γ_{11} above a certain w_{PEG} is associated with a decrease in the mobilities of the PEG molecules. Similar to the observation in Refs. [21] and [34], the decrease in the mobility might be caused by a more rigid structure in the liquid at higher w_{PEG}. However, detailed insights into the diffusion process taking into consideration the fluid structure on a molecular level can only be accessed with help of molecular dynamics simulations.

While the uncertainty in D_{11} generally decreases with increasing w_{PEG}, there are two exceptions for $w_{\mathrm{PEG}}=(0.300$ and $0.599)$ at $T=298$ K. For $w_{\mathrm{PEG}}=0.300$, two individual measurements were performed. While U_{r} in D_{11} for the first measurement is 2.1 %, for the second one for the same sample a larger uncertainty of 7.8 % could be found. This behavior can be due, for example, to incorrect alignment of the instrument, scratches on the surface of the cuvette, and additional contamination from sample handling. All these aspects have a negative impact on the recorded CFs in terms of lower SNR and excessive long-term noise, thus increasing uncertainties. For $w_{\mathrm{PEG}}=0.599$, i.e., close to the solubility limit, the relatively large U_{r} in D_{11} may be related to the unstable and inhomogeneous sample. This statement is supported by the observed precipitation in the sample after a certain time, if the sample remains untouched.

3.3.3 Temperature Dependence for Technical PEG 4000

D_{11} of the binary mixtures of water with technical PEG 4000 at $w_{\mathrm{PEG}}=0.01$ determined by DLS are given as a function of T in Fig. 6.

As expected, D_{11} increases with increasing T. It can be considered to follow a typical Arrhenius-type behavior, but the limited T range and the present uncertainties also allow other descriptions with, e.g., an exponential or second-order polynomial. Considering the corresponding temperature dependence of the dynamic viscosity of water, the calculated hydrodynamic diameters for the same system at different T via the Stokes–Einstein equation based on the determined D_{11} remain constant within the experimental uncertainties. This further supports the picture of the diffusion behavior of sphere-like PEG molecules resembling that of a particulate

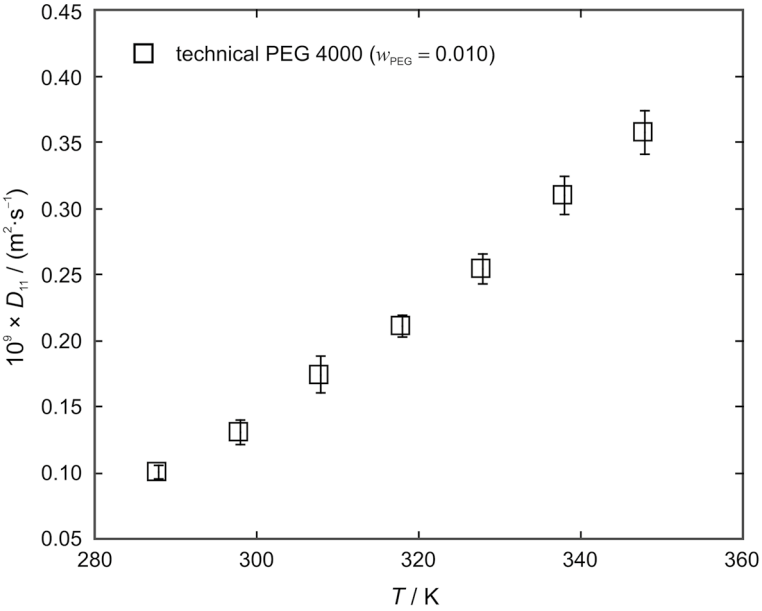

Fig. 6 Mutual diffusivity D_{11} of binary mixtures of water and technical PEG 4000 at $w_{PEG}=0.010$ determined by heterodyne DLS at temperatures ranging from (288 to 348) K. Expanded experimental uncertainties ($k=2$) are indicated by error bars

system. Thus, D_{11} can be considered as the translational diffusion coefficient or self-diffusion coefficient of sphere-like PEG molecules dissolved in water.

4 Conclusion

The present study demonstrates that the heterodyne DLS method can be successfully applied for the reliable determination of the mutual diffusivity D_{11} of binary mixtures of water with technical polydisperse PEGs with different molar masses as well as with a pure monodisperse PEG over a broad range of concentrations and temperatures. Considering all investigated systems and thermodynamic states, the expanded experimental uncertainty ($k=2$) in D_{11} ranges from (1.4 to 46.7) % and is 10.3 % on average, where the average reduces to 5.5 % for PEG mass fractions from 0.01 to 0.6. Excellent agreement with the available literature data can be found, where increasing molar mass of PEG leads to decreasing D_{11} values. From these results, it can be further deduced that within uncertainties, D_{11} determined in an aqueous system with pure monodisperse PEG agrees with that of such systems with technical polydisperse PEG with the corresponding central molar mass. While a typical increase in D_{11} with increasing temperature was observed for the system based on PEG 4000, the nonlinear dependence of D_{11} on the mass fraction of dissolved PEG 4000 may be related to the concentration dependence of the thermodynamic factor as it has been shown in the literature for systems exhibiting a similar

diffusivity behavior. Close to infinite dilution of PEG, the measured mutual diffusivity D_{11} can be related to the self-diffusivity of PEG molecules with a specific hydrodynamic diameter. This shows the similarities in the diffusion behaviors of the sphere-like dissolved PEG molecules in water and that of particulate systems at sufficiently low concentrations. Considering this information, it can be concluded that especially monodisperse PEGs may be used as model systems to gain a fundamental understanding of diffusive processes in particulate systems, including bimodal and also multimodal systems.

Acknowledgments The authors gratefully acknowledge funding of the Erlangen Graduate School in Advanced Optical Technologies (SAOT) by the Bavarian State Ministry for Science and Art.

Author Contributions WW prepared the samples, measured the refractive index and the mutual diffusivity, and wrote the main manuscript text. MS synthesized and characterized the pure PEG homolog with preparative and analytical chromatography as well as wrote the corresponding text in the manuscript. All authors reviewed the manuscript.

Funding Open Access funding enabled and organized by Projekt DEAL. This work was funded by the Deutsche Forschungsgemeinschaft (DFG, German Research Foundation)—Project-ID 416229255-SFB 1411.

Data Availability Not applicable.

Declarations

Conflict of interest The authors declare they have no competing interests as defined by Springer, or other interests that might be perceived to influence the results and/or discussion reported in this paper.

References

1. F.G. Calvo-Flores, M.J. Monteagudo-Arrebola, J.A. Dobado, J. Isac-García, Top. Curr. Chem. **376**, 18 (2018). https://doi.org/10.1007/s41061-018-0191-6
2. L. Shi, J. Zhang, M. Zhao, S. Tang, X. Cheng, W. Zhang, W. Li, X. Liu, H. Peng, Q. Wang, Nanoscale **13**, 10748 (2021). https://doi.org/10.1039/D1NR02065J
3. A.A. D'souza, R. Shegokar, Expert Opin. Drug Deliv. **13**, 1257 (2016). https://doi.org/10.1080/17425247.2016.1182485
4. H. Schellekens, W.E. Hennink, V. Brinks, Pharm. Res. **30**, 1729 (2013). https://doi.org/10.1007/s11095-013-1067-7
5. J.F. Campos, S. Berteina-Raboin, Catalysts **10**, 429 (2020)
6. F. Lima, J. Gouvenaux, L.C. Branco, A.J.D. Silvestre, I.M. Marrucho, Fuel **234**, 414 (2018). https://doi.org/10.1016/j.fuel.2018.07.043

7. J. Chen, S.K. Spear, J.G. Huddleston, R.D. Rogers, Green Chem. **7**, 64 (2005). https://doi.org/10.1039/B413546F
8. M. Vafaeezadeh, M.M. Hashemi, J. Mol. Liq. **207**, 73 (2015). https://doi.org/10.1016/j.molliq.2015.03.003
9. Z. Yu, S. Bo, H. Wang, Y. Li, Z. Yang, Y. Huang, Z.-X. Jiang, Mol. Pharm. **14**, 3473 (2017). https://doi.org/10.1021/acs.molpharmaceut.7b00496
10. K. Kinbara, Polym. J. **50**, 689 (2018). https://doi.org/10.1038/s41428-018-0074-2
11. A. Vergara, L. Paduano, V. Vitagliano, R. Sartorio, Phys. Chem. Chem. Phys. **1**, 5377 (1999). https://doi.org/10.1039/A906197E
12. K. Shimada, H. Kato, T. Saito, S. Matsuyama, S. Kinugasa, J. Chem. Phys. **122**, 244914 (2005). https://doi.org/10.1063/1.1948378
13. E. Feitosa, W. Brown, K. Wang, P.C.A. Barreleiro, Macromolecules **35**, 201 (2002). https://doi.org/10.1021/ma010696w
14. K.L. Linegar, A.E. Adeniran, A.F. Kostko, M.A. Anisimov, Colloid J. **72**, 279 (2010). https://doi.org/10.1134/S1061933X10020195
15. A.I. Norman, Y. Fei, D.L. Ho, S.C. Greer, Macromolecules **40**, 2559 (2007). https://doi.org/10.1021/ma0622783
16. M.L. Alessi, A.I. Norman, S.E. Knowlton, D.L. Ho, S.C. Greer, Macromolecules **38**, 9333 (2005). https://doi.org/10.1021/ma051339e
17. T. Gruendling, M. Guilhaus, C. Barner-Kowollik, Anal. Chem. **80**, 6915 (2008). https://doi.org/10.1021/ac800591j
18. M. Piszko, F.D. Lenahan, S. Hahn, M.H. Rausch, T.M. Koller, T. Klein, A.P. Fröba, J. Chem. Eng. Data **66**, 2218 (2021). https://doi.org/10.1021/acs.jced.1c00084
19. M. Piszko, T. Schaible, C. Bonten, A.P. Fröba, Macromolecules **54**, 5662 (2021). https://doi.org/10.1021/acs.macromol.1c00819
20. T. Klein, M. Piszko, C.J. Kankanamge, G. Kasapis, A.P. Fröba, J. Phys. Chem. B **125**, 5100 (2021). https://doi.org/10.1021/acs.jpcb.1c01616
21. W. Wu, T. Klein, M. Kerscher, M.H. Rausch, T.M. Koller, C. Giraudet, A.P. Fröba, J. Phys. Chem. B **124**, 2482 (2020). https://doi.org/10.1021/acs.jpcb.0c00646
22. C. Giraudet, M.S.G. Knoll, Y. Galvan, S. Süß, D. Segets, N. Vogel, M.H. Rausch, A.P. Fröba, Transp. Porous Med. **131**, 723 (2020). https://doi.org/10.1007/s11242-019-01364-1
23. F.E. Berger Bioucas, C. Damm, W. Peukert, M.H. Rausch, T.M. Koller, C. Giraudet, A.P. Fröba, J. Phys. Chem. B **123**, 9491 (2019). https://doi.org/10.1021/acs.jpcb.9b08274
24. A.P. Fröba, S. Will, Y. Nagasaka, J. Winkelmann, S. Wiegand, W. Köhler, In *Experimental Thermodynamics Volume IX: Advances in Transport Properties of Fluids*, (The Royal Society of Chemistry, 2014), p. 19–74
25. B.J. Berne, R. Pecora, *Dynamic Light Scattering: With Applications to Chemistry, Biology, and Physics* (Dover Publications, Mineola, 2013)
26. L. Onsager, Phys. Rev. **37**, 405 (1931). https://doi.org/10.1103/PhysRev.37.405
27. A.V. Malm, J.C.W. Corbett, Sci. Rep. **9**, 13519 (2019). https://doi.org/10.1038/s41598-019-50077-4
28. M. Piszko, W. Wu, S. Will, M.H. Rausch, C. Giraudet, A.P. Fröba, Fuel **242**, 562 (2019). https://doi.org/10.1016/j.fuel.2019.01.078
29. W. Wu, T. Klein, M. Kerscher, M.H. Rausch, T.M. Koller, C. Giraudet, A.P. Fröba, J. Phys. Chem. B **123**, 8777 (2019). https://doi.org/10.1021/acs.jpcb.9b06211
30. A. Einstein, Ann. Phys. **322**, 549 (1905). https://doi.org/10.1002/andp.19053220806
31. M.L. Huber, R.A. Perkins, A. Laesecke, D.G. Friend, J.V. Sengers, M.J. Assael, I.N. Metaxa, E. Vogel, R. Mareš, K. Miyagawa, J. Phys. Chem. Ref. Data **38**, 101 (2009). https://doi.org/10.1063/1.3088050
32. C.J. Fee, J.M. Van Alstine, Bioconjug. Chem. **15**, 1304 (2004). https://doi.org/10.1021/bc049843w
33. A. Vergara, L. Paduano, G. D'Errico, R. Sartorio, Phys. Chem. Chem. Phys. **1**, 4875 (1999). https://doi.org/10.1039/A905035C
34. T. Klein, W. Wu, M.H. Rausch, C. Giraudet, T.M. Koller, A.P. Fröba, J. Phys. Chem. B **122**, 7122 (2018). https://doi.org/10.1021/acs.jpcb.8b03568
35. G. Guevara-Carrion, T. Janzen, Y.M. Muñoz-Muñoz, J. Vrabec, J. Chem. Phys. **144**, 124501 (2016). https://doi.org/10.1063/1.4943395
36. D. Zabala, C. Nieto-Draghi, J.C. de Hemptinne, A.L. López de Ramos, J. Phys. Chem. B **112**, 16610 (2008). https://doi.org/10.1021/jp8042329